Ansal, A. M., Krizek, R. J., and Bažant, Z.P. (1981). "Prediction of soil behavior by endochronic theory." Proc., *Workshop on Limit Equilibrium, Plasticity and Generalized Stress-Strain in Geotechnical Engineering*, held at McGill Univ. May 1980, ed. by R. K. Yong, and H.-Y. Ko, ASCE, New York 256–327.

Proceedings of the Workshop on

Limit Equilibrium, Plasticity and Generalized Stress-Strain In Geotechnical Engineering

McGill University
May 28-30, 1980

Sponsored by:
National Science Foundation, U.S.A.
National Science and Engineering Research Council, Canada
McGill University
Univ. of Colorado

Raymond K. Yong and Hon-Yim Ko, Workshop Co-Chairmen

Published by the
American Society of Civil Engineers
345 East 47th Street
New York, New York 10017

published 1981

PREDICTION OF SOIL BEHAVIOR BY ENDOCHRONIC THEORY

by

Atilla M. Ansal[1], A. M. ASCE

Raymond J. Krizek[2], M. ASCE

Zdeněk P. Bažant[2], M. ASCE

[1]Assistant Professor of Geotechnical Engineering, Macka Civil Engineering Faculty, Istanbul Technical University, Istanbul, Turkey.

[2]Professor of Civil Engineering, The Technological Institute, Northwestern University, Evanston, Illinois, U.S.A.

INTRODUCTION

The ultimate usefulness of any particular constitutive relationship is dictated in large part by a proper balance among (a) the versatility of the theory to characterize experimental data obtained from a variety of different tests, (b) the ability of the resulting relationship to predict behavior for conditions other than those which were used to "calibrate" the model, and (c) the ease with which the formulation can be adopted to the solution of practical boundary value problems. Exercises in fitting data and predicting response patterns therefore provide valuable comparisons among different theories and serve to identify and clarify the advantages and disadvantages of each.

However, when undertaking such comparisons, it must be recognized that most data sets are rather limited and frequently do not include the types of tests that would be required to pass judgment on the fundamental hypotheses and concepts of various constitutive models, and this is indeed the case here. As explained in a companion paper (5), a proper comparison of the basic ideas underlying different constitutive models would require (a) tests for which the stress path in stress space is highly nonproportional, including "loading to the side" (which is difficult to achieve experimentally), and (b) tests which involve unloading and cyclic loading. Since such data are not included in the set provided for this study, it will be impossible to adequately evaluate the validity and utility of various theories. In fact, the predictions requested for this study are primarily interpolations between extreme cases that were given for the same type of test, rather than for a basically different type of test.

In particular, the selected types of tests comprise a data set that happens to be unfavorable for an examination of endochronic theory and favors

other theories. This is because endochronic theory was developed primarily to represent the response for unloading and cyclic loading and is most effective in such cases. Other theories which were developed mainly to model monotonic proportional loading response are favored by the data set provided and their performance under conditions of cyclic loading is not tested. This must be taken into account when forming judgments on the relative merits of the various theories based on the present data set. For the types of tests used (which do not include "loading to the side" or cyclic loading), it is, in principle, possible to adequately describe all of the given data and obtain reasonable predictions with nearly all available theories, and the closeness of the fits and predictions is largely a measure of the skill, intuition, experience, and persistence of the predictor rather than the features of the model.

SUMMARY OF BASIC EQUATIONS

The basic concept of endochronic theory is that of an intrinsic time scale, which is formulated to account for the dissipative effects of inelastic strain. Intrinsic time is defined as a monotically increasing scalar function of strain and time, and one suitable definition (9) is

$$(dz)^2 = \left[\frac{d\zeta}{z_1}\right]^2 + \left[\frac{dt}{\tau_1}\right]^2 \tag{1a}$$

$$d\zeta = F(\underline{\varepsilon}, \underline{\zeta})\, d\xi \tag{1b}$$

$$d\xi = \sqrt{\tfrac{1}{2}\, de_{ij}\, de_{ij}} \tag{c}$$

where ε_{ij} is the strain tensor in cartesian coordinates $x_i (i = 1,2,3)$; z_1 and τ_1 are constant material parameters; $e_{ij} = \varepsilon_{ij} - \delta_{ij}\varepsilon$ is the deviator of ε_{ij};

$\varepsilon = \varepsilon_{kk}/3$ is the volumetric (mean) strain; δ_{ij} is Kronecker delta; and F is a strain hardening-softening function.

Assuming that the source of inelasticity in soils is the irreversible rearrangement of grain configurations associated with deviatoric strains, it is convenient to characterize the accumulation of grain rearrangements by an appropriate variable, ζ, termed the rearrangement measure, which is expressed in terms of the distortion measure, ξ, as given in Equations 1b and 1c. Since the increments of irreversible (inelastic) strain are caused by interparticle rearrangements, they must be proportional to the increments of the rearrangement measure, and the proportionality coefficient may, in general, depend on both the state of stress and strain. However, it has been observed in both quasi-static and cyclic tests (2,7) that these irreversible rearrangements diminish with the number of cycles. To express this phenomenon, it is suitable to consider the strain hardening-softening relationship as a composite function, such as

$$F(\underline{\varepsilon}, \underline{\zeta}, \zeta)d\xi = d\eta/f(\eta) \tag{2a}$$

$$d\eta = F_\eta(\underline{\varepsilon}, \sigma)d\xi \tag{2b}$$

The introduction of a new parameter, η, in terms of the function F, adjusts the rate of accumulation of inelastic strains, and the function $f(\eta)$ serves as a hardening function which causes a stiffening of the response for repeated loading (that is, contraction of hysteresis loops and an increase of their slope as the number of load cycles increases).

INTRINSIC MATERIAL FUNCTIONS

The forms of the material functions are assumed to be the same for both isotropic and anisotropic soils, and the anisotropy is accounted for by

replacing the stress and strain invariants in these relationships with the appropriate transversely isotropic or orthotropic invariants (3). The material functions were introduced so as to reflect various obvious governing factors. In particular, F_η is assumed to have the form (1, 2).

$$F_\eta(\underset{\sim}{\varepsilon}, \underset{\sim}{\sigma}) = F_{\eta 1}(I_1^\varepsilon)F_{\eta 2}(I_1^{\bar{\sigma}})F_{\eta 3}(J_2^\varepsilon) \tag{3}$$

Since a change in interparticle distances, reflected as a change in volume, must result in a change in both deviatoric and volumetric stiffnesses, the softening-hardening function should increase as the volume increases. Thus, $F_{\eta 1}$ may be expressed in terms of the first strain invariant as $F_{\eta 1}(I_1^\varepsilon) = |1 - a_1 I_1^\varepsilon|$, in which a_1 is a positive material parameter. The frictional aspect of soils suggests that the deviatoric strain softening and hardening should depend on the effective confining stress, and this dependency is achieved by using the first invariant of the effective stress in the from $F_{\eta 2}(I^{\bar{\sigma}}) = [0.01 + a_2(I_1^{\bar{\sigma}}/P_a)]^{-1}$, in which a_2 is a positive material parameter and p_a is atmospheric pressure (expressed in the same units as the stress invariant and introduced to achieve a dimensionless relationship). The effects of shear strains are introduced into the relationship in terms of the second deviatoric strain invariant, J_2^ε, in the form $F_{\eta 2}(J_2^\varepsilon) = 1 + a_3 J_2^\varepsilon$, in which a_3 is a material parameter.

Aside from the foregoing factors that control strain softening and hardening, there is an upper limit for softening and hardening, and this upper limit depends on the accumulated inelastic strains but seems to be essentially independent of the factors that cause them. This limit corresponds to what is known as the critical state, for which both strain hardening and strain softening diminish. A general limiting relation which incorporates this phenomenon can be formulated in terms of the accumulated grain rearrangements, and this formulation is developed by considering another variable, η, which represents continuous rearrangements, such that

$$d\eta = \left[a_0 + \frac{|1 - a_1 I_1^\varepsilon|(1 + a_3 J_2^\varepsilon)}{0.01 + a_2(I_1^{\bar{\sigma}}/p_a)}\right] d\xi \tag{4}$$

in which a is a positive material parameter that is necessary to determine the irreversible strain increment for the critical case (where there is no hardening or softening). This limiting function is chosen as

$$f(\eta) = 1 + \beta_1 \eta/(1 + \beta_2 \eta) \tag{5}$$

in which β_1 and β_2 are positive material parameters that depend on the stress history.

Most soils also manifest inelastic volumetric strains, termed densification or dilatancy, as a result of shear. It is assumed here that the inelastic volume changes due to shear and those due to changes in the hydrostatic stress can be treated separately. The inelastic volume change (volumetric strain) due to shear is denoted λ and is called the densification and dilatancy measure. It can be expressed as a function of the stress and strain invariants and the accumulated value of λ as follows:

$$d\lambda = L(\underset{\sim}{\varepsilon}, \underset{\sim}{\sigma}, \lambda)d\xi , \tag{6}$$

The major factors affecting dilatancy and densification can be expressed as

$$L(\underset{\sim}{\varepsilon}, \underset{\sim}{\sigma}, \lambda) = L_1(I_1^\varepsilon)L_2(I_1^{\bar{\sigma}})L_3(J_2^\varepsilon)L_4(\lambda). \tag{7}$$

Following arguments similar to those outlined for the strain hardening-softening relationship, the increment of inelastic volumetric strain due to shear can be expressed as

$$d\lambda = \left[\frac{C_0\left(1 + C_1 I_1^{\xi}\right)}{(1 + C_2 I_1^{\bar{\sigma}}/P_a)(1 + C_3 J_2^{\xi})(1 + C_4\lambda)}\right] d\xi \tag{8}$$

in which coefficients C_i are material parameters. Inelastic volume changes are also produced by changes in the effective volumetric stress. This phenomenon is taken into account by defining a second intrinsic time, $\bar{z}$, which involves a term called the compaction measure, $\bar{\xi}$, that is expressed in terms of volumetric strains as

$$d\bar{\xi} = \left|d\epsilon_1 + d\epsilon_2 + d\epsilon_3\right| \tag{9a}$$

$$(d\bar{z})^2 = \left[\frac{d\bar{\xi}}{z_2}\right]^2 + \left[\frac{dt}{\tau_2}\right]^2 \tag{9b}$$

$$d\bar{\zeta} = d\bar{\eta}/h(\bar{\eta}) \tag{9c}$$

$$d\bar{\eta} = H(\underset{\sim}{\sigma})d\bar{\xi} \tag{9d}$$

in which $h(\bar{\eta})$ is the compaction hardening function and $H(\underset{\sim}{\sigma})$ is the compaction softening function. Following a line of reasoning similar to that outlined before, Equation 9d can be written in an analogous form (8), where

$$d\bar{\eta} = \frac{b_1\left|I_1^{\bar{\sigma}}/P_a\right|}{1 + b_2\left|I_1^{\bar{\sigma}}/P_a\right|}\, d\bar{\xi} \tag{10a}$$

$$h(\bar{\eta}) = 1 + b_3\bar{\eta} + b_4\bar{\eta}^2 \tag{10b}$$

in which b_1, b_2, b_3, and b_4 are constant material parameters.

The concept of a two-phase medium is a natural choice for analyzing the undrained behavior of saturated soils. Since the compressibility of the soil grains is about thirty times less than the compressibility of water, the assumption of incompressible soil grains will not introduce any significant

error. On the other hand, the fluid phase (pore water) must be treated as compressible, and the solid structure (matrix of soil particles) is even more compressible than the pore water. The tendency of the solid structure to change volume is coupled with the pore pressure, and the solid structure will deform only as much as the pore water permits. If no drainage is allowed, the volume change of the solid structure will equal the volume change of the pore fluid, and the total volumetric strain of the pore water can be expressed in terms of the total volumetric strain of the soil structure; thus, the pore pressure increment can be expressed as (1, 2)

$$du = B_w(d\epsilon_1 + d\epsilon_2 + d\epsilon_3)/n \tag{11}$$

where n is the porosity of the soil and B_w is the bulk modulus of water.

The variations of the elastic moduli along the stress path are taken into consideration and formulated as functions of the initial magnitudes of the moduli and the ratios of the changes that take place in certain important parameters. Two major factors that change along a given stress path are the void ratio and the effective normal stress. These variables, in turn, depend on the accumulated densification-dilatancy measure, λ, and the first effective stress invariant, which is adopted to represent the change in the elastic moduli, and all of the independent elastic moduli are expressed in the form (1)

$$E_r = E_o\left[1 + M_1(I_1^{\bar{\sigma}} - I_1^{\bar{\sigma}_o})/I_1^{\bar{\sigma}_o} + 3M_2\lambda_r/n\right] \tag{12}$$

where E_o is the initial modulus; $I_1^{\bar{\sigma}_o}$ is the initial first effective stress invariant; and M_1 and M_2 are empirically determined material constants which are assumed here to be 0.1.

STRESS-STRAIN RELATIONS

The endochronic constitutive model was originally developed for isotropic soils (2, 4, 6), and the stress-strain relations involved only two independent elasticity coefficients; however, it appears more realistic to consider most soils to be transversely isotropic or orthotropic. An endochronic constitutive model for transversely isotropic clays has been developed (3) and involves five elasticity coefficients. This approach is extended here to model the behavior of orthotropic soils and the following stress-strain relations are proposed

$$d\epsilon_{11} = c_{11}d\bar{\sigma}_{11} + c_{12}d\bar{\sigma}_{22} + c_{13}d\bar{\sigma}_{33} + d\epsilon'_{11} \quad (13a)$$

$$d\epsilon_{22} = c_{12}d\bar{\sigma}_{11} + c_{22}d\bar{\sigma}_{22} + c_{23}d\bar{\sigma}_{33} + d\epsilon'_{22} \quad (13b)$$

$$d\epsilon_{33} = c_{13}d\bar{\sigma}_{11} + c_{23}d\bar{\sigma}_{22} + c_{33}d\bar{\sigma}_{33} + d\epsilon'_{33} \quad (13c)$$

$$d\epsilon_{12} = c_{44}d\sigma_{12} + d\epsilon'_{12} \quad (13d)$$

$$d\epsilon_{13} = c_{55}d\sigma_{13} + d\epsilon'_{13} \quad (13e)$$

$$d\epsilon_{23} = c_{66}d\sigma_{23} + d\epsilon'_{23} \quad (13f)$$

Here, superimposed bars denote effective stresses; $\bar{\sigma}_{ij}$ are components of the effective stress tensor; ϵ_{ij} are the strain components; ϵ'_{ij} are components of the inelastic strains; and c_{ij} are elasticity coefficients. The inelastic strain increments are assumed to have the same form as previously derived for transversely isotropic soils (3) and are introduced as

$$d\epsilon'_{11} = D_1(\bar{\sigma}_{11}-\bar{\sigma}_{22})dz + D_2(\bar{\sigma}_{11}-\bar{\sigma}_{33})dz + d\epsilon''/(1 + r_1 + r_2) \quad (14a)$$

$$d\epsilon'_{22} = D_1(\bar{\sigma}_{22}-\bar{\sigma}_{11})dz + D_3(\bar{\sigma}_{22}-\bar{\sigma}_{33})dz + r_1 d\epsilon''/(1 + r_1 + r_2) \quad (14b)$$

$$d\epsilon'_{33} = D_2(\bar{\sigma}_{33}-\bar{\sigma}_{11})dz + D_3(\bar{\sigma}_{33}-\bar{\sigma}_{22})dz + r_2 d\epsilon''/(1 + r_1 + r_2) \quad (14c)$$

$$d\epsilon_{12} = c_{44}\sigma_{12}dz \quad (14d)$$

$$d\epsilon_{13} = c_{55}\sigma_{13}dz \quad (14e)$$

$$d\epsilon_{23} = c_{66}\sigma_{23}dz \quad (14f)$$

where it is assumed that $D_1 = c_{44}/3$, $D_2 = c_{55}/3$, and $D_3 = c_{66}/3$; coefficients r_1 and r_2 characterize anisotropy; and $d\epsilon''$ represents the inelastic volume change, expressed as

$$d\epsilon'' = d\lambda + \frac{\bar{\sigma}}{3K}d\bar{z} \quad (15)$$

where $d\lambda$ is the inelastic volume change increment due to deviatoric distortion and $(\bar{\sigma}d\bar{z}/3K)$ is the inelastic volume change due to a change in the effective volumetric stress. The stress-strain relations for the simpler case of a transversely isotropic soil are listed in the Appendix.

FITTING OF TEST DATA

When fitting test data with the foregoing constitutive equations, the test specimens are assumed to be in a homogeneous state of stress and strain. Due to the complex nature of the differential equations, a step-by-step process is employed and strains or stresses are increased in small increments. Values from each previous step provide initial estimates, and inner iterations within a step are used to obtain improved response increments within the step. For the initial iteration of the first loading increment, all incremental values must be estimated (can be taken as zero). Experience indicates that this step-by-step integration method is reasonably stable, and, provided loading steps are sufficiently small, convergence is usually achieved after a couple of iterations for strain-controlled tests. For the stress-controlled tests

convergence is also achieved after a couple of iterations during the initial stage of loading, but, as the stress-strain curve approaches its peak point, it is necessary to decrease the loading increment continuously in order to prevent instability.

The final form of the equations and the values of the material parameters were obtained by using a mathematical optimization procedure to minimize the differences between observed and calculated responses. A finite difference Levenberg-Marquart subroutine for solving nonlinear least squares problems (developed by T. J. Aird of International Mathematical and Statistical Library package) was utilized for this purpose. Due to the complex nonlinear form of the constitutive relations, it is probably possible to have different sets of material parameter values that give fairly good results; however, the optimization routine only identifies local optimums in the vicinity of the initial estimates.

Due partly to the versatility of endochronic theory and partly to the large number of material parameters used in the constitutive relations, it is always possible to get fairly accurate fits (2, 3, 7). However, the purpose here was to find a set of values which would give reasonable fits for all of the given stress paths and which would yield logical correlations with material properties and the stress and strain state of the soil. This set is not necessarily the global optimum. Many stages of optimization were required to determine the effects of different parameters and to achieve realistic fits and correlations. Although the process of accomplishing this task is based somewhat on previous knowledge about the behavior of soils and the characteristics of the model, it is still largely a trial-and-error procedure.

EXPRESSIONS FOR DATA FITS

Essentially four different soils were investigated in this study.

The first two were sensitive clays which appear to have very similar index properties; however, the tests were performed under different initial confining stresses such that the overconsolidation ratio, p/p_o, was less than unity for one of the clays. For these two clays, which were termed "X" and "Y", the reported response indicated anisotropy with respect to all three axes. To be able to model such a behavior it was necessary to extend the previously developed formulation to handle orthotropic stress-strain relations, which require nine elasticity coefficients. The expressions were developed using arguments previously outlined for transversely isotropic soils (3).

The third soil was a laboratory prepared kaolinite clay which was assumed to be transversely isotropic due to the K_o consolidation that was used in sample preparation. The fourth soil was a dry Ottawa sand, which also showed transversely isotropic response in one test (which was the only test that could reflect this property of the sand). The transversely isotropic stress-strain relation outlined in the Appendix was adopted to predict the stress-strain behavior.

Even though these four soil types are very different from one another, all of the given test data were modeled by using the same material functions, and no attempt was made to modify the general form of the material relationships to improve the accuracy of the fits for each type of soil separately. This demonstrates the generality and versatility of the endochronic constitutive equations. The chosen material functions are given below in incremental form:

$$d\eta = \left[4 + \frac{\left| 1 - 500\, I_1^{\epsilon} \right| (1 + a_d J_2^{\epsilon})}{0.01 + 0.75\, I_1^{\bar{\sigma}}/P_a} \right] d\xi \,, \qquad (16)$$

$$dz = \frac{d\eta}{z_1 \left[1 + \beta_1 \eta/(1 + \beta_2 \eta) \right]} , \tag{17}$$

$$d\lambda = \frac{c_1 \left| 1 + 2500\ I_1^{\varepsilon} \right|}{(1 + 3000\ J_2^{\varepsilon})(1 + 0.25 I_1^{\bar{\sigma}}/P_a)(1 + c_2\lambda)} \tag{18}$$

$$d\bar{\eta} = \frac{b \left| I_1^{\bar{\sigma}}/P_a \right|}{1 + \left| I_1^{\bar{\sigma}}/P_a \right|} d\xi , \tag{19}$$

$$d\bar{z} = \frac{d\bar{\eta}}{z_2 (1 + 2500\bar{\eta} + 1000\bar{\eta}^2)} \tag{20}$$

Only eight soil-specific material parameters were used to model the given test data; all others were held constant for all soils and all stress or strain histories. These eight parameters were initially determined separately for each test; then, trial-and-error procedures were employed to identify a suitable set that would yield realistic fits for all of the tests performed under the same consolidation stress, and the predictions were based on these values.

ANALYSIS OF TEST DATA

Clays X and Y

As mentioned earlier, orthotropic stress-strain relations were used to model the behavior of these clays; these relations required nine elasticity coefficients and two material coefficients to define the appropriate stress-strain invariants. An attempt was made to decrease the number of elasticity coefficients by assuming that (a) values for Poisson's ratio in all three directions are equal ($\mu_{21} = \mu_{32} = \mu_{31}$) and the other values in the corresponding planes (μ_{12}, μ_{23}, μ_{13}) can be determined from the symmetry condition of the stiffness matrix, and (b) compression and shear moduli in the minor and intermediate principal planes can be expressed in terms of compression and shear moduli in the major plane, where the proportionality constants are the same for both moduli. With these assumptions it was possible to express elasticity coefficients in terms of five parameters as

$$\mu_{21} = \mu_{32} = \mu_{31} = \mu \tag{21}$$

$$E_2 = r_1 E_1 \ ; \quad E_3 = r_2 E_1 \tag{22}$$

$$G_2 = r_1 G_1 \ ; \quad G_3 = r_2 G_1 \tag{23}$$

where G is the shear modulus; E is the compression modulus; μ is Poisson's ratio; and r_1 and r_2 are proportionality constants which characterize the anisotropy of the material. The variations of the major principal elastic moduli, E_1 and G_1, along a particular stress path were formulated as given by Equation 12, and variations of the other moduli were calculated by Equations 22 and 23.

It was also necessary to express the strain and stress invariants with two proportionality constants in order to include the effect of anisotropy and establish invariance with respect to the orthogonal transformations. As in the case of transversely isotropic clays (3), it was assumed that the first stress invariant retains the same form and the strain invariants are defined in terms of two proportionality constants as

$$I_1^{\varepsilon} = \varepsilon_1 + r_3\varepsilon_2 + r_4\varepsilon_3 \tag{24}$$

$$J_2^{\varepsilon} = \left[(\varepsilon_1 - r_3\varepsilon_2)^2 + (\varepsilon_1 - r_4\varepsilon_3)^2 + (r_3\varepsilon_2 - r_4\varepsilon_3)^2 \right] \Big/ 6 \tag{25}$$

where $r_3 = 1/r_1$ and $r_4 = 1/r_2$. With the introduction of two proportionality or anisotropy constants (r_1, r_2), three elasticity coefficients (E_1, G_1, μ), and

eight material constants (a_d, b, c_1, c_2, z_1, z_2, β_1, β_2), thirteen constants must be determined.

The curves shown in Figure 1 for Clay X were obtained by fitting each test separately; however, every effort was made to hold most of the material parameters constant for the entire data set, and only four (c_1, c_2, E_1, z_1) of the thirteen parameters were allowed to vary within a limited range. The values of the constant and variable parameters used to obtain the fits are summarized in Table 1.

Table 1. Variable and Constant Material Parameters for Clay X

Constant material parameters: a_d = 380, β_1 = 24; β_2 = 5; b = 0.1; z_2 = 50,000; r_1 = 0.8; r_2 = 0.9; G_1/P_a = 48; μ = 0.18

Variable material parameters:

		z_1	E_1/P_a	c_1	c_2
σ_c = 10 psi	m = 0	0.0696	88	0.7500	30,000
	m = 1	0.0861	88	0.7500	230,000
σ_c + 20 psi	m = 0	0.0600	88	0.7500	500
	m = 1	0.0660	30	0.0021	230,000
σ_c = 30 psi	m = 0	0.0600	34	0.7500	500
	m = 1	0.1140	29	0.0021	230,000

As can be seen from the given curves, the stress-strain fits are reasonably good, but the model generally yields smaller volumetric strains. It is believed that this is partially a result of keeping certain parameters constant, as given in Equations 16 to 20, because the model was originally developed for normally consolidated clays. In the case of sensitive clays the collapse of the soil structure appears to give large volumetric strains and a more linear stress-strain response in the initial portion followed by a sudden increase in strain. Unlike normally consolidated insensitive clays, there appears to be a distinct yield point. Due to the flexibility of endochronic theory, it is possible to model the stress-strain behavior of sensitive clays very accurately, but it may be necessary to increase the range of the variable parameters or to change the values of the constants and even the functional forms of the material relationships given in Equations 16 to 20.

After the workshop at McGill University, an attempt was made to improve some of the fits for Clay X. As shown typically in Figure 2, it was possible to obtain excellent fits for the first two tests performed at σ_c = 10 psi, but there were large variations in the values of some of the variable parameters, even for the two tests considered. This suggests the need to modify some of the material relationships to handle sensitive clays. The curves given in Figure 2 were calculated by changing only the values of the four variable parameters given in Table 1 to the values presented in Table 2, while keeping all others constant and equal to their values given in Table 1.

Table 2. Variable Parameters Used for Improved Fits for Clay X

		z_1	E_1/P_a	c_1	c_2
σ_c = 10 psi	m = 0	0.038	77	0.750	30,000
	m = 1	1800	26	0.091	30,000

In the case of Clay Y the curves shown in Figure 3 were obtained by optimizing the fits with respect to the four variable parameters given in Table 2 to get the values summarized in Table 3, while keeping all others equal to their values given in Table 1. The model appears to give better results for Clay Y than for Clay X, but there are still large differences between observed and calculated volumetric strains. The initial fits shown in Figure 4 can be compared to the improved fits shown in Figure 3a to evaluate the degree of improvement that has been achieved. As can be seen, a major improvement was realized in modeling the volumetric change.

Table 3. Variable Parameters Used for Improved Fits for Clay Y

		z_1	E_1/P_a	c_1	c_2
σ_c = 2.5 psi	m = 0	0.026	136	0.042	30,000
	m = 1	0.042	129	0.007	30,000
σ_c = 5 psi	m = 0	0.028	133	1.970	30,000
	m = 1	0.046	111	0.660	30,000
σc = 10 psi	m = 0	0.060	681	0.750	500
	m = 1	0.060	681	0.750	500

The stress-strain curves shown in Figures 5 and 6 are typical predicted tests results for Clays X and Y, respectively. These predictions have been obtained by using the same material parameters used in the initial predictions, the only difference between these curves and those presented at the workshop being that the loading was stopped as soon as strain softening started, because the tests were stress-controlled. Due to an error in the computer program, strain hardening previously occurred at this point, and this deficiency was corrected prior to obtaining the new plots.

Kaolinite Clay

A transversely isotropic stress-strain relation was adopted for the kaolinite clay because samples were subjected to K_o consolidation before they were sheared. It is generally accepted that K_o consolidation will result in some particle reorientation, which is a cause of anisotropy. In the case of transversely isotropic soils, five elasticity coefficients are needed. However, expressing these coefficients in terms of ratios makes it possible to decrease this number. As in the case of orthotropic soils, it is assumed here that (a) Poisson's ratio in all planes is the same ($\mu_{21} = \mu_{13} = \mu_{23} = \mu$), and (b) the compression modulus, E_1 in the plane of isotropy can be expressed in the terms of the compression modulus in the vertical direction, E_3, in the form $E_1 = r_1 E_3$. As a result, the number of elasticity coefficients may be reduced to three (μ, E_1, G_{32}), and r_1 is the proportionality parameter representing the degree of anisotropy. The transversely isotropic strain invariants may be expressed (3) as

$$I_1^{\epsilon} = \epsilon_{11} + \epsilon_{22} + r_2\,\epsilon_{33} \tag{26}$$

$$J_2^{\epsilon} = \left[(\epsilon_{11}-\epsilon_{22})^2 + (\epsilon_{11}-r_2\epsilon_{33})^2 + (\epsilon_{22}-r_2\epsilon_{33})^2\right]/6 + \epsilon_{12}^2 + r_3(\epsilon_{13}^2+\epsilon_{23}^2) \tag{27}$$

where i = 3 represents the direction perpendicular to the plane of isotropy; r_3 is a proportionality constant; and $r_2 = (c_1 + c_2 + c_4)/(c_3 + 2c_4)$, where c_i are the elasticity coefficients, as given in the Appendix. The value for r_2 is determined by use of the assumption that hydrostatic stress changes will not produce any distortional inelastic strains (3). In the case of transversely isotropic soils the proposed constitutive model requires three elasticity coefficients (μ, E_1, G_{32}), three proportionality parameters (r_1, r_3, r_4), and eight material constants (a_d, b, c_1, c_2, z_1, z_2 θ_1 β_2), where r_4 is incorporated into the constitutive equations as shown in the Appendix.

These parameters were determined by trial and error, and the optimization technique was used to get fits for the compression tests with one set of numbers and fits for the extension tests with another set of numbers. Without further complications it was not possible to incorporate into the formulation the differences in the test data between compression and extension tests and obtain a single set of parameters for all four tests. It also was not possible to obtain the shear modulus, G_{32}, in the plane of anisotropy because no torsional test data were given; hence, G_{32} was estimated from the observed degree of anisotropy and other elasticity moduli. The values of the material constants obtained from the given compression and extension test data are summarized in Table 4.

Table 4. Optimized Parameters for Kaolinite Clay

Tests	a_d	β_1	β_2	z_1	c_1	c_2	E_3/P_a	r_1	r_4
1 & 4	5.0	3.84	6.65	0.01660	1.4800	41,000	709	0.68	0.51
10 & 13	12.0	1.50	5.00	0.00914	0.0012	2,000	386	0.98	1.42

Note: For all tests b = 0.5, μ = 0.21, z_2 = 10,000, and r_3 = 0.57.

The main reason for the differences in the parameters shown in Table 4 is probably due to the difference in the behavior of kaolinite in compression and tension, and it was not possible to handle this phenomenon with the present formulation. The optimized curves for the given test data are shown in Figure 7, and the predictions are shown in Figures 8, 9, 10, and 11. The predictions were based on the average values of the parameters given in Table 4, but, since the behavior is so different in tension and compression, it did not appear realistic to use one value for the elasticity coefficient E_3. Instead, E_3 was calculated separately for each test with respect to the inclination of the stress path compared to the stress path in a standard compression test by using a quarter of an ellipse. The ellipse was drawn with its minor radius as E_3 from extension tests and its major radius as E_3 obtained from compression tests. Then, E_3 for the test was determined graphically by measuring the appropriate radius of the ellipse. The value of the shear modulus, G_{32}, was estimated from the values for E_3.

Ottawa Sand

As mentioned previously, transversely isotropic constitutive relations were used to model the tests on dry Ottawa sand. In particular, the same material relationships were adopted to demonstrate the flexibility of the approach, and, even though sensitive Clay X and dry Ottawa sand manifest different behavioral patterns, it was possible to obtain realistic fits for the data supplied on both soils.

The data set included tests with unloading and reloading cycles. Based on the method explained earlier, jump-kinematic hardening was incorporated into the formulation in terms of the deviatoric component of the stress tensor. This was accomplished by defining the deviatoric stresses as

$$\bar{s}_{ij} = s_{ij} - \alpha_{ij} \tag{28}$$

and

$$d\bar{z} = c_u dz \tag{29}$$

where α_{ij} and c_u must be redefined at each load reversal point. For the given test data $c_u = 1$ and $\alpha_{ij} = 0$ for virgin loading, $c_u = 0.5$ and $\alpha_{ij} = s_{ij_{max}}$ for unloading, and $c_u = 0.7$ and $\alpha_{ij} = 0$ for reloading, because loading and reloading started from the hydrostatic stress state. Even though jump-kinematic hardening is in essence just an empirical technique to improve the model, it also reflects some of the salient features found in the stress-strain behavior of soil under repeated loading. Most soils manifest considerable inelastic response in the loading branch, but their response is much more elastic upon unloading; hence, it is logical to decrease the value of the intrinsic time increment, dz, since it is the controlling factor for accumulating plastic strains. On the other hand, it has been observed that the response in the reloading branch up to the previous maximum stress level is more or less elastic, after which the stress-strain behavior continues almost on the path obtained in the virgin loading branch. Therefore, it appears logical to reset c_u and α_{ij} at these points.

The fits were obtained by using trial-and-error and the optimization scheme, and values of the parameters and constants are summarized in Table 6.

Table 6. Material Parameters Used to Obtain Fits for Ottawa Sand

	c_1	a_d	β_1	β_2	z_1	E_3/P_a	G_{32}/P_a	r_3	r_4
σ_c = 5 psi									
CTC m = 0	0.000720	0.800	3.8	5	0.00280	1034	748	0.80	1.3
TE m = 1	0.000720	0.800	3.8	5	0.00330	517	340	0.80	0.8
σ_c = 10 psi									
CTC m = 0	0.000014	1.230	3.8	28	0.00510	1177	953	0.50	1.3
TC m = 0	0.000014	1.230	3.8	28	0.00510	1177	953	0.35	1.3
TE m = 1	0.000014	2.500	3.8	28	0.00510	1177	953	0.20	1.3
σ_c = 20 psi									
TC m = 0	0.000014	0.034	20.0	5	0.00556	734	510	0.80	0.8
TE m = 1	0.057700	0.048	20.0	5	0.00313	374	210	0.80	0.8

Constants: $\mu = 0.3$; $c_2 = 2{,}000$; $b = 0.01$; $z_2 = 1.7 \times 10^6$

As can be seen, it was possible to obtain the fits shown in Figures 12, 13, and 14 by changing the values of only a few parameters. However, in the case of Ottawa sand it appears necessary with the present intrinsic relationships to have different sets of values for the material parameters for each confining stress. The predictions shown in Figures 15 to 21 were calculated by using a different average set of material parameters for each confining stress, with estimates being based on the values in Table 6.

APPENDIX

STRESS-STRAIN RELATIONS FOR TRANSVERSELY ISOTROPIC SOILS

When the soil is transversely isotropic, the constitutive relations simplify to the form:

$$d\varepsilon_{11} = c_1 d\bar{\sigma}_{11} + c_2 d\bar{\sigma}_{22} + c_4 d\bar{\sigma}_{33} + d\varepsilon'_{11} \quad \text{(A-1)}$$

$$d\varepsilon_{22} = c_2 d\bar{\sigma}_{11} + c_1 d\bar{\sigma}_{22} + c_4 d\bar{\sigma}_{33} + d\varepsilon'_{22} \quad \text{(A-2)}$$

$$d\varepsilon_{33} + c_4 d\bar{\sigma}_{11} + c_4 d\bar{\sigma}_{22} + c_3 d\bar{\sigma}_{33} + d\varepsilon'_{33} \quad \text{(A-3)}$$

$$d\varepsilon_{12} = (c_1 - c_2) d\sigma_{12} + d\varepsilon'_{12} \quad \text{(A-4)}$$

$$d\varepsilon_{23} = c_5 d\sigma_{23} + d\varepsilon'_{23} \quad \text{(A-5)}$$

$$d\varepsilon_{13} = c_5 d\sigma_{13} + d\varepsilon'_{13} \quad \text{(A-6)}$$

Here superimposed bars denote effective stresses; ε_{ij} are components of total strains; ε'_{ij} are components of inelastic strains; and c_i are elasticity coefficients. Equations A-1 to A-6 are referred to cartesian axes x_1, x_2 and x_3, of which x_3 is normal to the plane of isotropy. The inelastic strain increments can be given as

$$d\varepsilon'_{11} = D_1(\bar{\sigma}_{11} - \bar{\sigma}_{22})dz + D_2(\bar{\sigma}_{11} - \bar{\sigma}_{33})dz + (1 - r_4)d\varepsilon'' \quad \text{(A-7)}$$

$$d\varepsilon'_{22} = D_1(\bar{\sigma}_{22} - \bar{\sigma}_{11})dz + D_2(\bar{\sigma}_{22} - \bar{\sigma}_{33})dz + (1 - r_4)d\varepsilon'' \quad \text{(A-8)}$$

$$d\varepsilon''_{33} = D_2(\bar{\sigma}_{33} - \bar{\sigma}_{11})dz + D_2(\bar{\sigma}_{33} - \bar{\sigma}_{22})dz + (1 + 2r_4)d\varepsilon'' \quad \text{(A-9)}$$

$$d\varepsilon'_{12} = (c_1 - c_2)\sigma_{12}dz \quad \text{(A-10)}$$

$$d\varepsilon'_{13} = c_5\sigma_{13}dz \quad \text{(A-11)}$$

$$d\varepsilon'_{23} = c_5\sigma_{23}dz \quad \text{(A-12)}$$

where $D_1 = (c_1 - c_2)/3$, $D_2 = (c_3 - c_4)/3$, r_4 is an anisotropy coefficient, and $d\varepsilon^{\cdot}_{\cdot}$ represents the inelastic volume change as given by Equation 15.

REFERENCES

1. Ansal, A. M. (1977), "An Endochronic Constitutive Law for Normally Consolidated Cohesive Soils," Ph.D. Dissertation, Department of Civil Engineering, Northwestern University, Evanston, Illinois, 166 pp.

2. Ansal, A. M., Bažant, Z. P. and Krizek, R. J. (1979), "Viscoplasticity of Normally Consolidated Clays," Journal of the Geotechnical Engineering Division, American Society of Civil Engineers, Volume 105, Number GT4, pp. 519-537.

3. Bažant, Z. P., Ansal, A. M. and Krizek, R. J. (1979), "Viscoplasticity of Transversely Isotropic Clays," Journal of the Engineering Mechanics Division, American Society of Civil Engineers, Volume 105, Number EM4, pp. 549-569.

4. Bažant, Z. P. and Krizek, R. J. (1976), "Endochronic Constitutive Law for Liquefaction of Sand," Journal of the Engineering Mechanics Division, American Society of Civil Engineers, Volume 102, Number EM2, pp. 225-238.

5. Bažant, Z. P., Ansal, A. M. and Krizek, R. J. (1980), "Critical Appraisal of Endochronic Theory for Soils," Proceedings of Workshop on Constitutive Modeling of Soils," McGill University, Montreal, Canada.

6. Cuellar, V., Bažant, Z. P., Krizek, R. J. and Silver, M. L. (1977), "Densification and Hysteresis of Sand under Cyclic Shear," Journal of the Geotechnical Engineering Division, American Society of Civil Engineers, Volume 103, Number GT5, pp. 399-416.

7. Krizek, R. J., Ansal, A. M. and Bažant, Z. P. (1978), "Constitutive Equation for Cyclic Behavior of Cohesive Soils," Geotechnical Engineering Division, Proceedings of the Specialty Conference on Earthquake Engineering and Soil Dynamics, American Society of Civil Engineers, Volume 2, pp. 557-568.

8. Sener, C. (1979), "An Endochronic Nonlinear Inelastic Constitutive Law for Cohesionless Soils Subjected to Dynamic Loading," Ph.D. Dissertation, Department of Civil Engineering, Northwestern University, Evanston, Illinois.

9. Valanis, K. C. (1971), "A Theory of Viscoplasticity Without a Yield Surface; Part I. General Theory; Part II. Application to Mechanical Behavior of Metals," Archives of Mechanics (Archiwum Mechaniki Stosowanej), Volume 23, pp. 517-555.

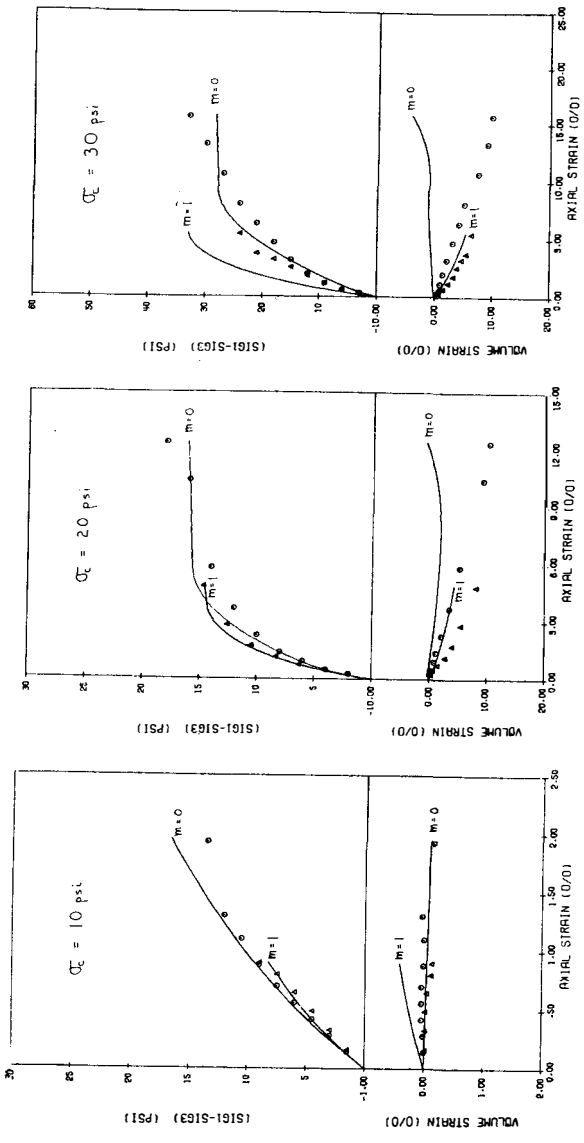

Figure 1. Initial Fits for Clay X

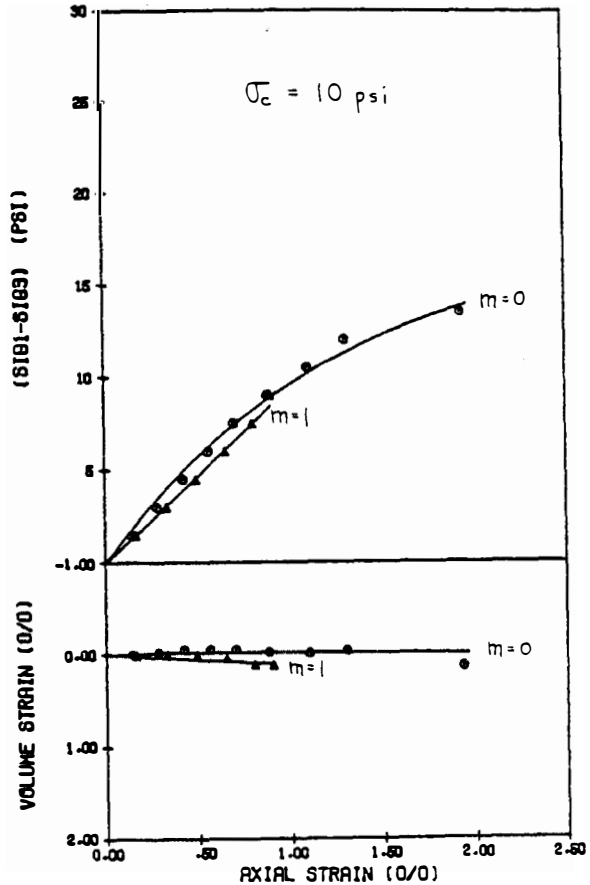

Figure 2. Improved Fits for Clay X

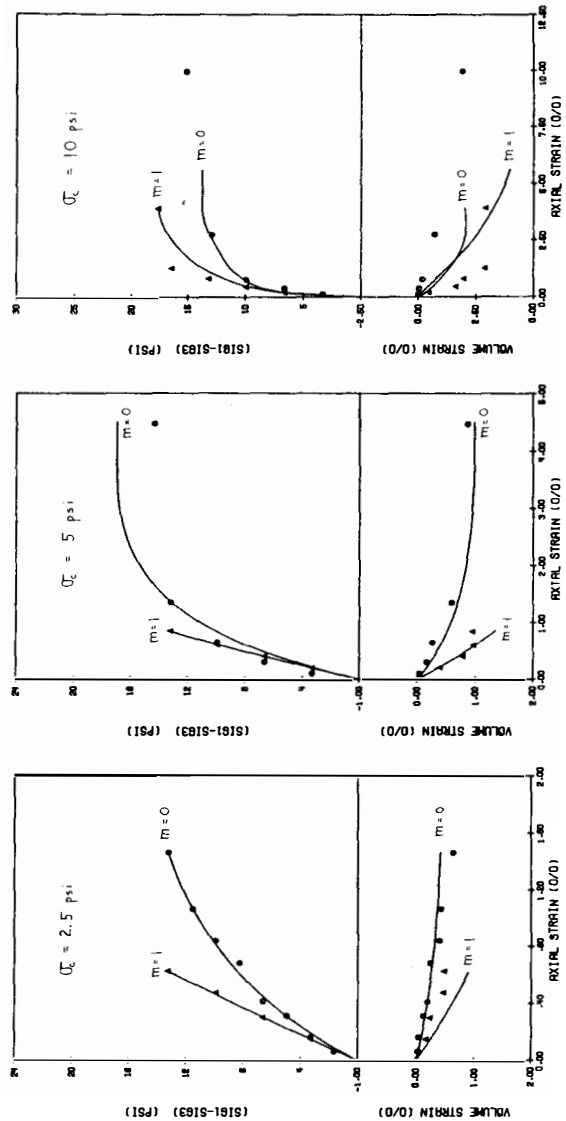

Figure 3. Improved Fits for Clay Y

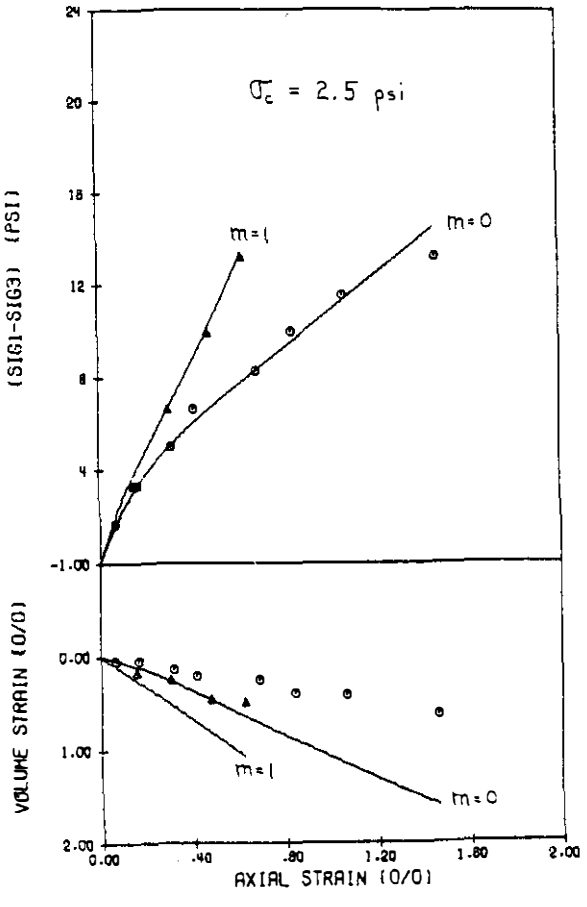

Figure 4. Initial Fits for Clay Y

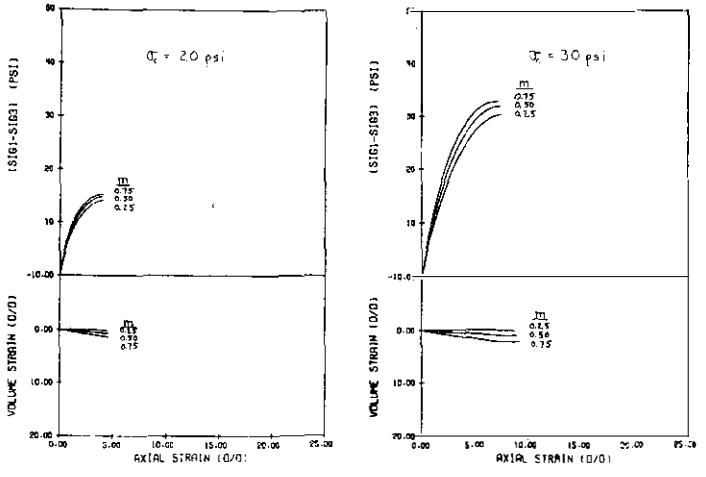

Figure 5. Typical Predictions for Clay X

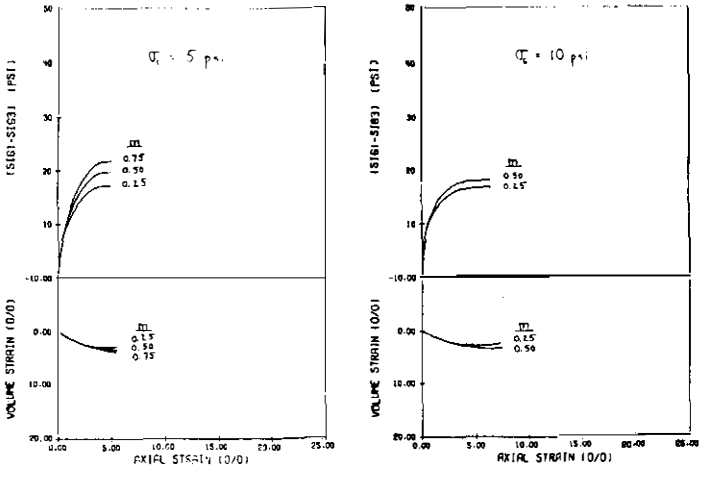

Figure 6. Typical Predictions for Clay Y

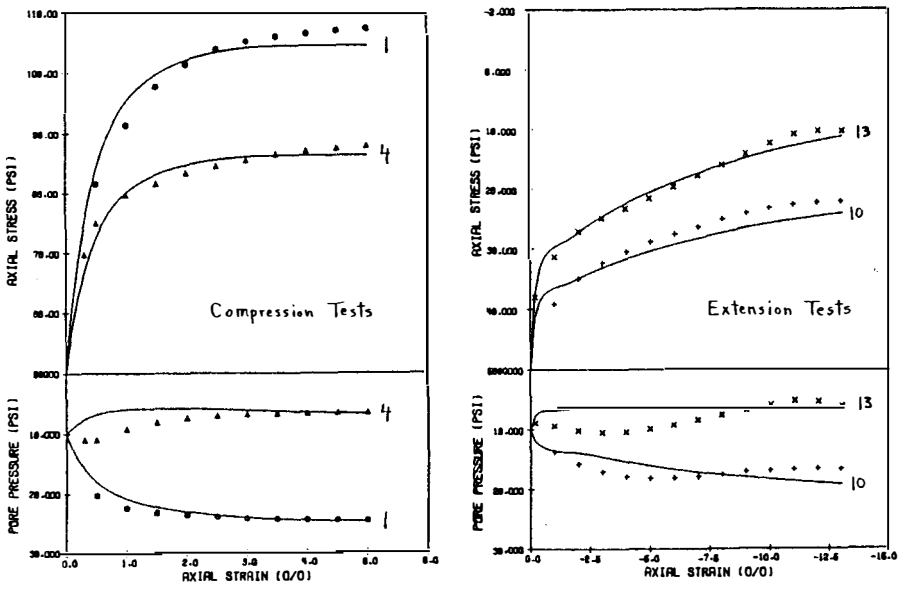

Figure 7. Optimized Fits for Kaolinite

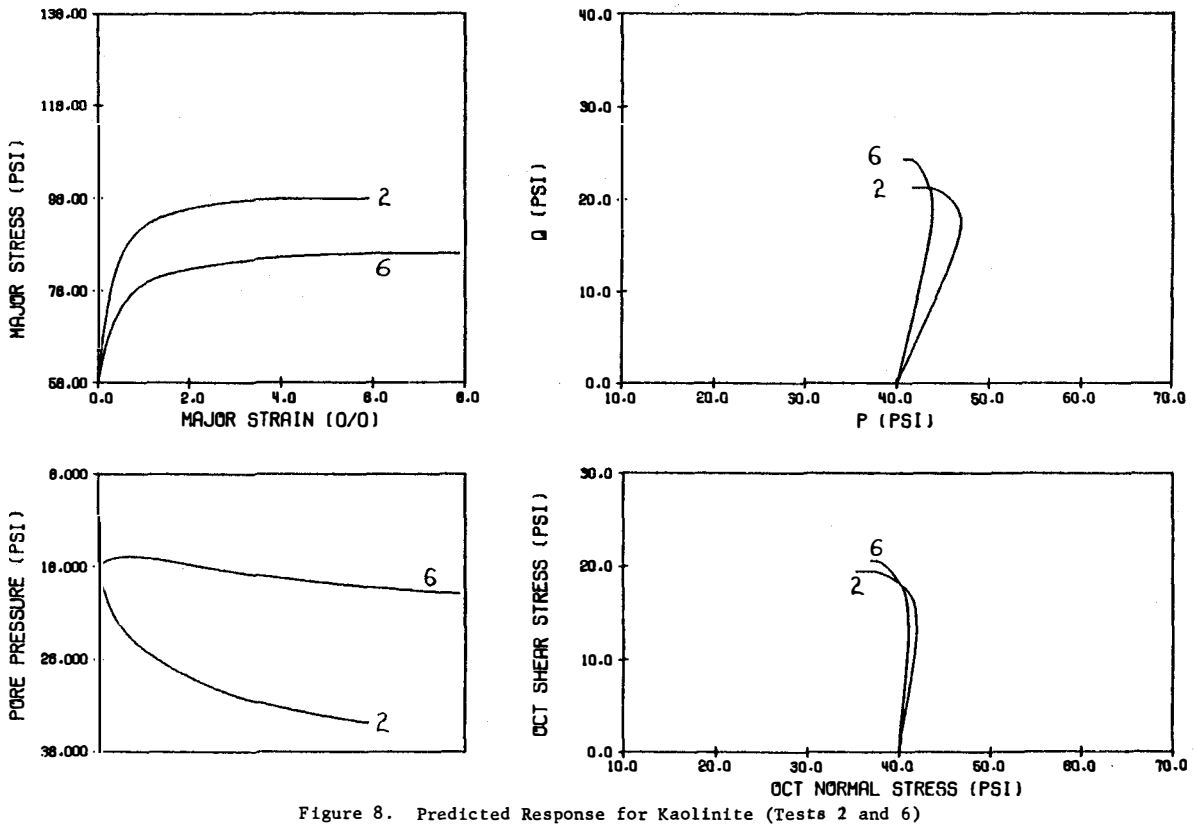

Figure 8. Predicted Response for Kaolinite (Tests 2 and 6)

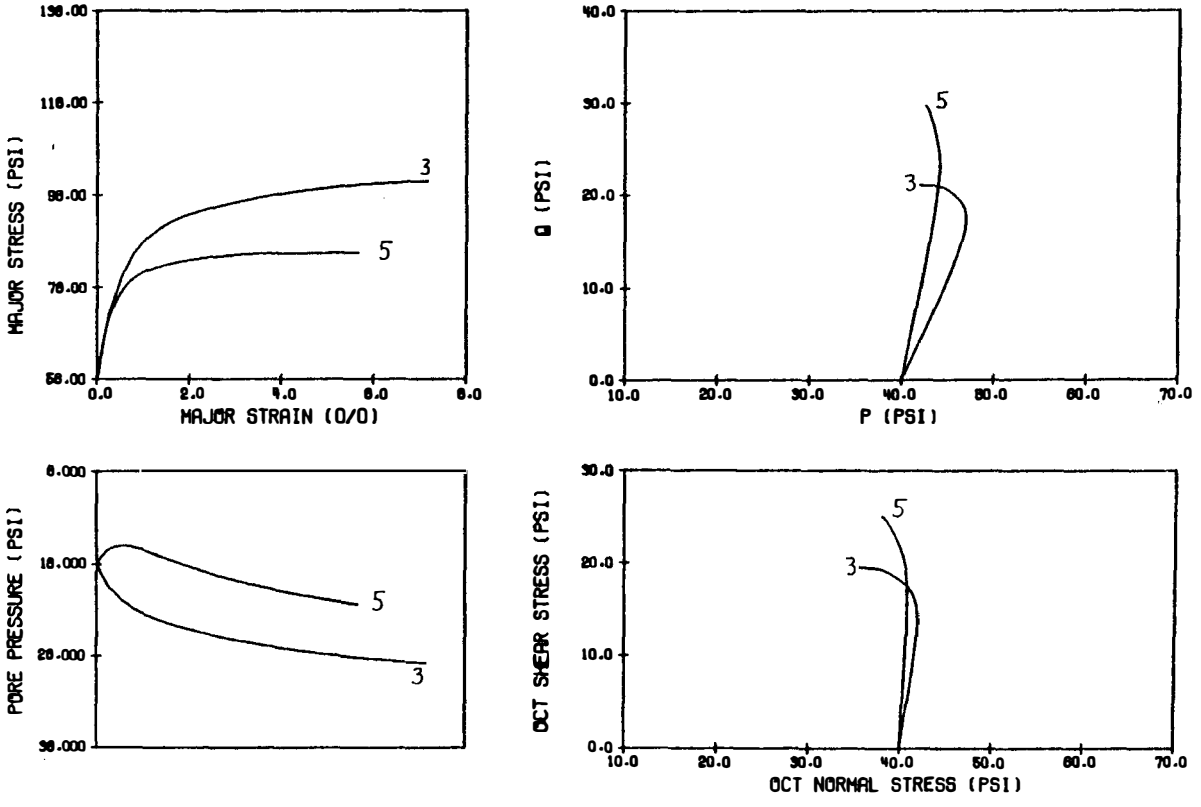

Figure 9 Predicted Response for Kaolinite (Tests 3 and 5)

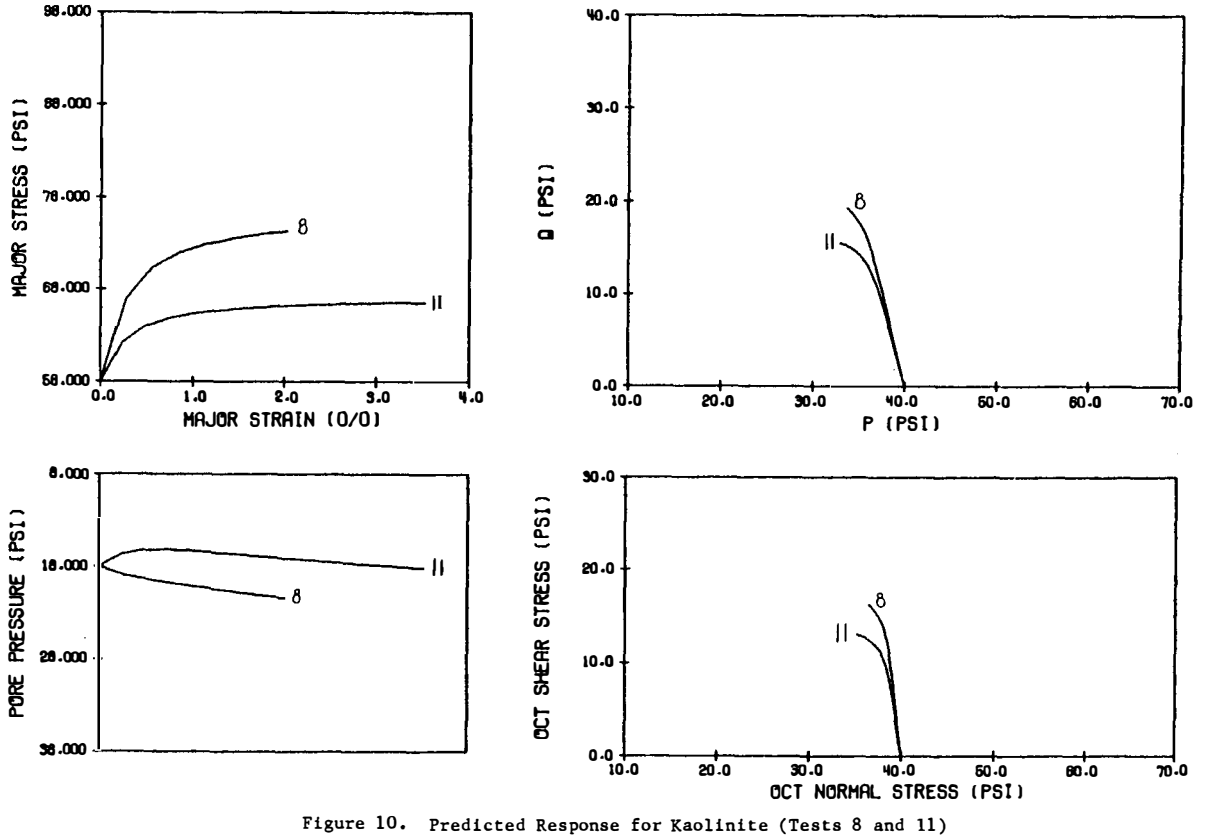

Figure 10. Predicted Response for Kaolinite (Tests 8 and 11)

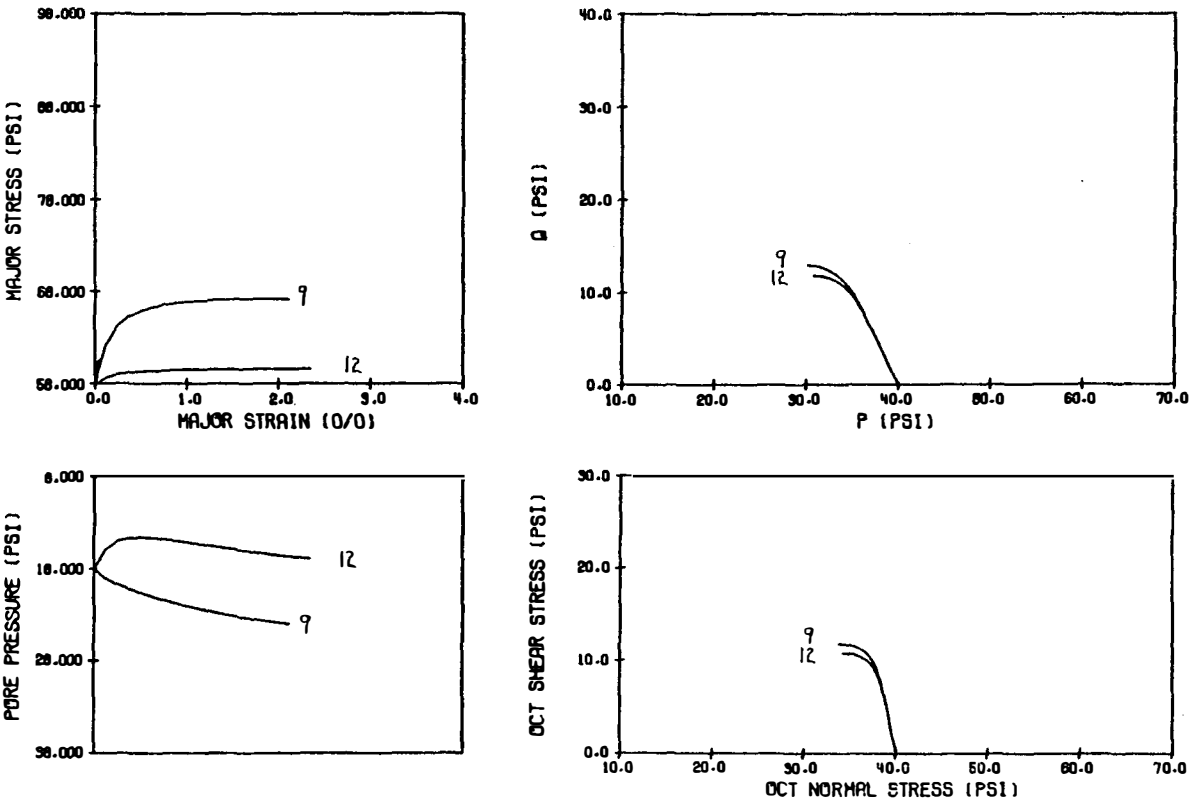

Figure 11. Predicted Response for Kaolinite (Tests 9 and 12)

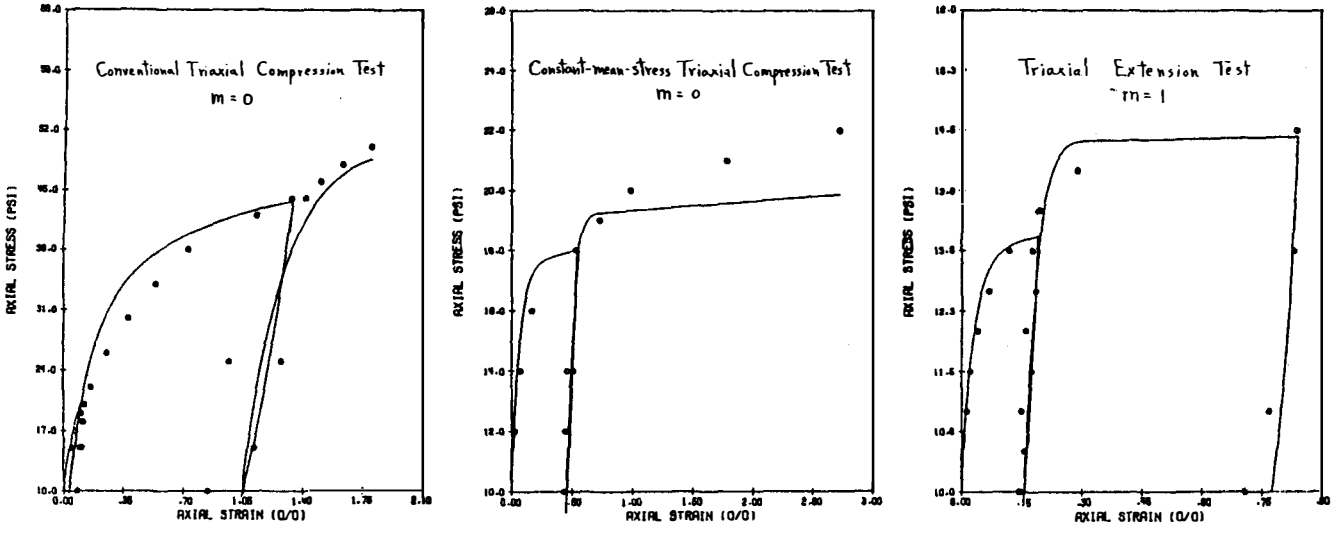

Figure 12. Optimized Fits for Ottawa Sand (Confining Stress = 10 psi)

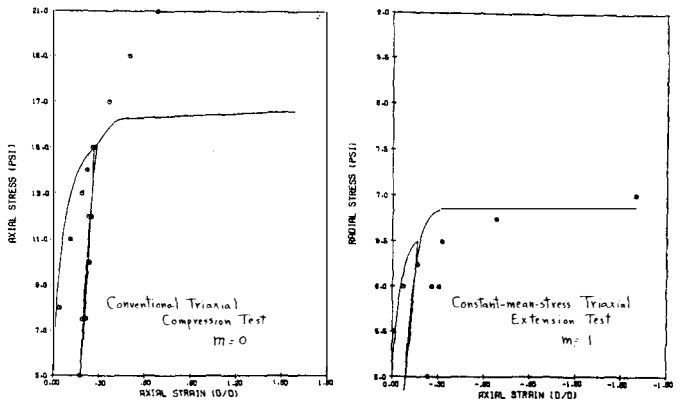

Figure 13. Optimized Fits for Ottawa Sand (Confining Stress = 5 psi)

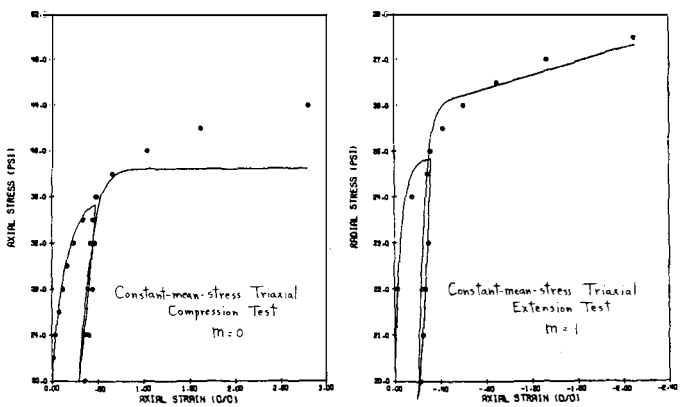

Figure 14. Optimized Fits for Ottawa Sand (Confining Stress = 20 psi)

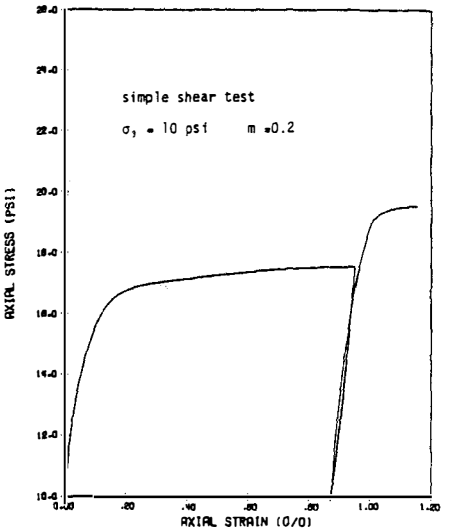

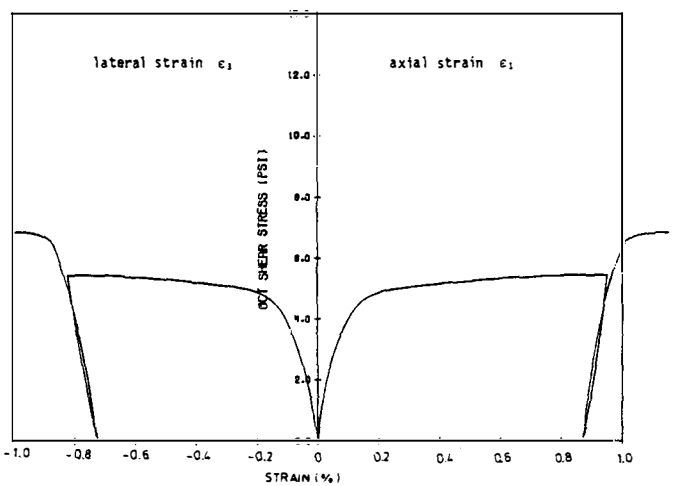

Figure 15. Predicted Response for Ottawa Sand in Simple Shear (Mean Stress = 10 psi; m = 0.2)

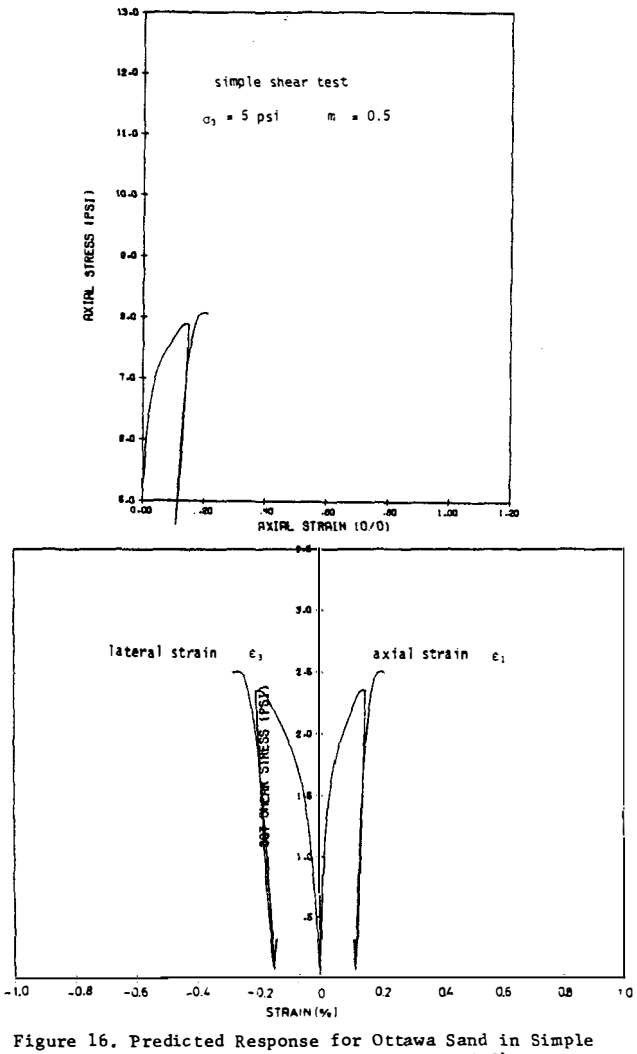

Figure 16. Predicted Response for Ottawa Sand in Simple Shear (Mean Stress = 5 psi; m = 0.5)

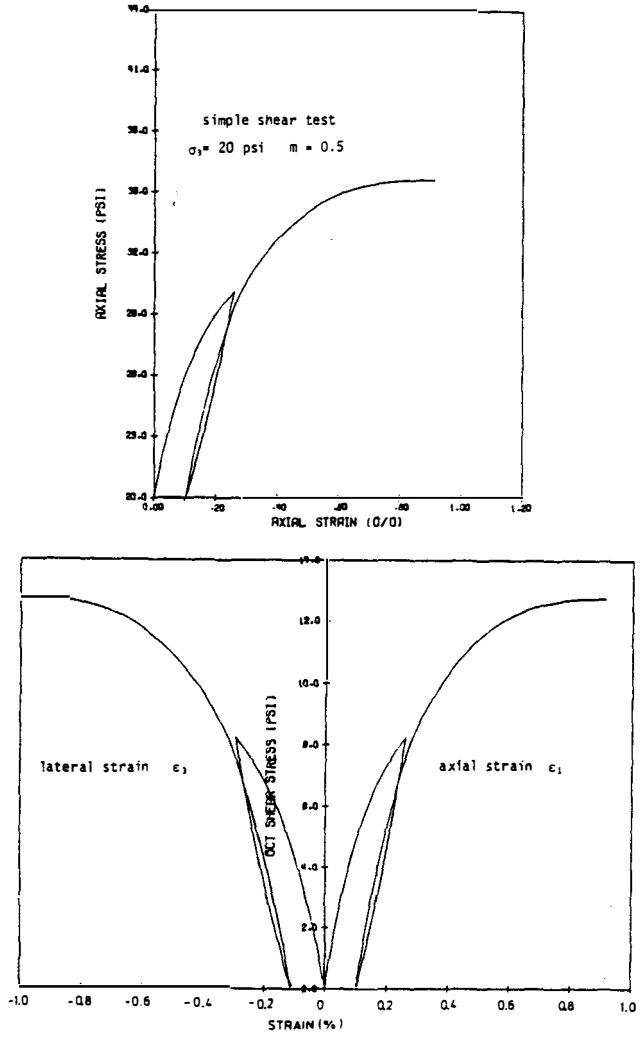

Figure 17. Predicted Response for Ottawa Sand in Simple Shear (Mean Stress = 20 psi; m = 0.5)

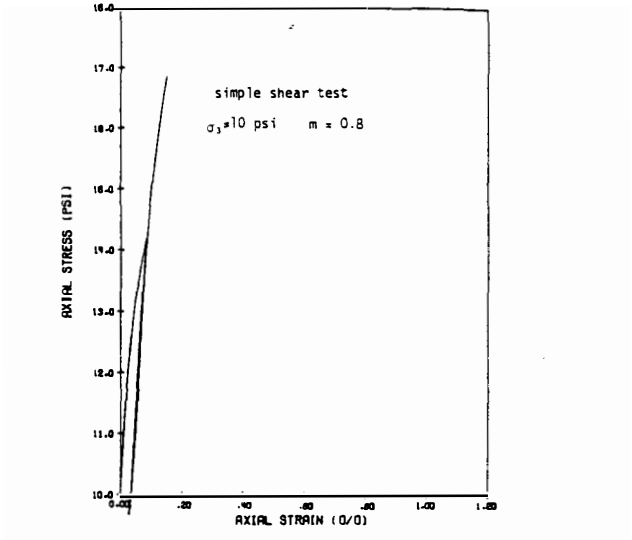

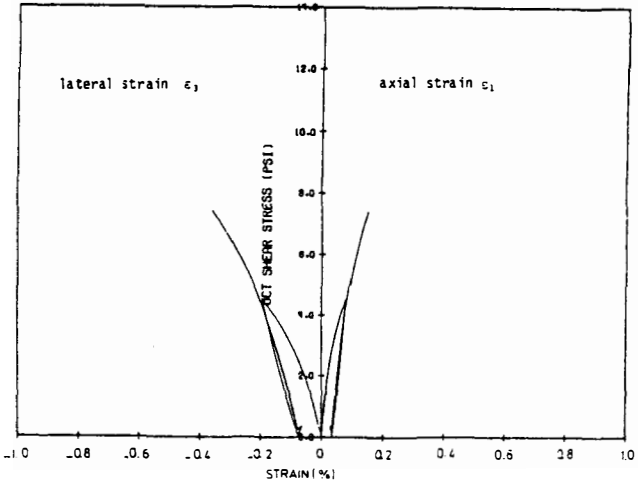

Figure 18. Predicted Response for Ottawa Sand in Simple Shear (Mean Stress = 10 psi; m = 0.8)

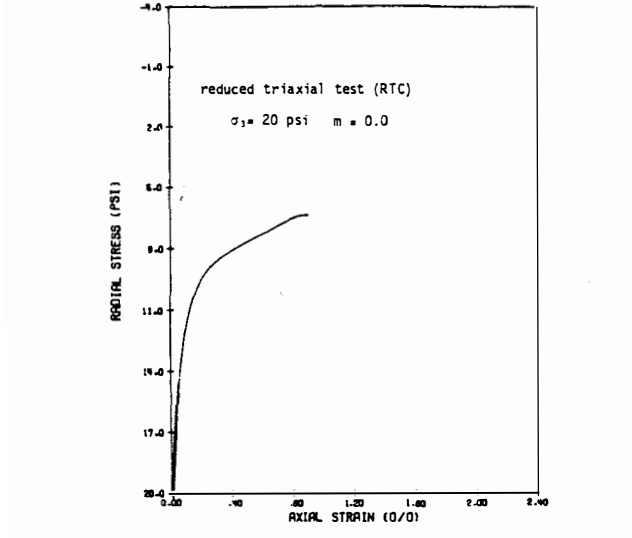

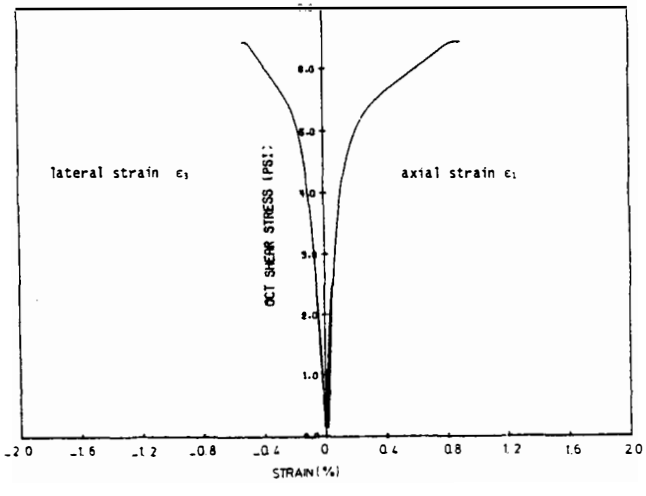

Figure 19. Predicted Response for Ottawa Sand in Reduced Triaxial Compression (Mean Stress=20 psi; m = 0)

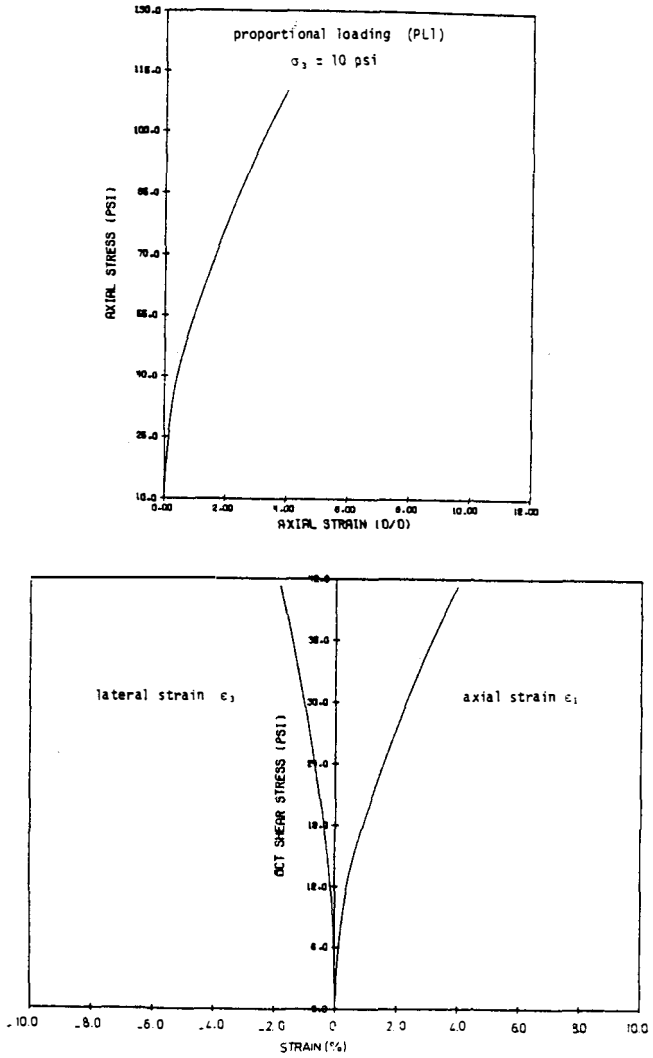

Figure 20. Predicted Response for Ottawa Sand Subjected to Proportional Loading PL 1 (Mean Stress = 10 psi; m = 0)

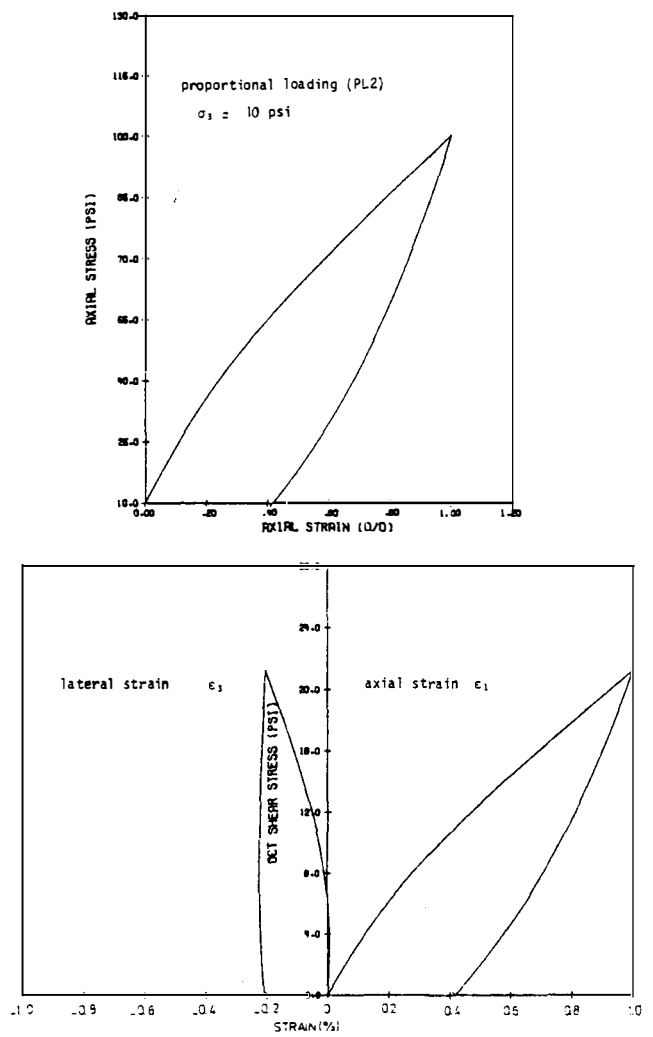

Figure 21. Predicted Response for Ottawa Sand Subjected to Proportional Loading PL 2 (Mean Stress = 10 psi; m = 0)